Wavelength insensitive fused fiber coupler in asymmetric heating of arc discharge

ARINDAM BISWAS[a*], B. K. RAY[a], HIMANSHU[a], C. KONER[b], S. CHAKRABORTY[a], K. N. HUI[c]
[a]*Dept. of ECE and EEE, NSHM Knowledge Campus, Arrah, Shibtala, Via Muchipara, Durgapur 713 212India*
[b]*Dept. of CSE, Dr. B C Roy Engineering College, Jemua Road, Fuljhore, Durgapur, West Bengal 713206*
[c]*Institute of Applied Physics and Materials Engineering, University of Macau, Avenida da Universidade, Taipa, Macau, China*

We demonstrate wavelength insensitive fused fiber couplers, obtained by multiple arc discharge around the coupler waist of two similar 2×2 SM fiber couplers in the temperature profile region. Placing the Coupler waist away from the arc flame produces the control temperature profile and hence phase mismatch between the fibers. Theoretically, the propagation constants are found out considering effective core diameters, core dopant diffusion, and coupling coefficient around the coupler waist. Variation of refractive index around the coupler waist with the number of arc discharge, and also depending on the position of the coupler waist from the centre of the arc flame, is shown. This helps to control wavelength insensitive characteristics of the component. A theoretical model for splitting ratio (SR) versus wavelength with repeated discharges producing increased phase mismatch and considering temperature profile parameters is developed. The theoretical curves are compared with the experimental results. For the particular fused coupler the wavelength insensitive ranging from 1.35μ*m* to 1.70μ*m* with maximum SR variation of 1.32*dB* at repeated discharge of D = 4 , were obtained.

(Received November 2, 2015; accepted November 25, 2016)

Keywords: 2×2 fused fiber couplers, Refractive index variation of the coupler waist in the arc discharge, Core dopant diffusion, Wavelength insensitive fused fiber couplers

1. Introduction

Optical fiber devices are important in-line components for optical communications and optical measurements. Normally, the optical fibers used to fabricate optical couplers have similar spectral characteristics so that the refractive index difference between core and cladding is almost constant against wavelength. Fused fiber couplers are used in many applications of optical networks and are fabricated by using a single-mode fiber Y junction [1], a Mach-Zehnder interferometer with two fused fiber couplers [2,3], two identical dispersive fibers whose index differences increase with wavelength or by producing asymmetry in the coupling region. The asymmetry within the coupling region was obtained by two dissimilar fibers [4], or by bending a fused fiber coupler [5], by prepolishing [6], etc. However, a novel method to fabricate fused fiber couplers by using two similar fibers with unequal heating by arc discharge is shown experimentally [7,8]. A temperature profile forming due to unequal heating in the two identical fibers of the coupler waist produces unequal index changes in the cores and claddings of the fibers around the coupling zone. Actually, the rapid cooling in arc discharge induces asymmetrically index changes in the coupling region of the two fibers and hence produces two average propagation constants of the respective modes of the two fibers in the coupling zone. In this paper, we demonstrate wavelength insensitive 2×2 fused fiber couplers. The coupling region of earlier made fused coupler was heated unequally by arc discharge when the coupling zone was placed a little away from the center of the arc flame to obtain a temperature profile, and was cooled rapidly. The temperature profile of the arc produces glass structure variation in the transverse direction of the coupling zone and forms a refractive index profile (Fig.6). The index profiles and their variations with arc temperature depending on arc current and arc time are estimated and the relation of propagation constant difference ($\Delta\beta$) of the fibers with the profile parameter ($D1$) in the coupling zone is shown. Variation of refractive indices n_{PD} of two cores with the position P=2*and*5 and four claddings (P=1,3,4 *and* 6) of two fibers around the coupler waist depending on both the number of arc discharge D and the position of the coupler waist from the centre of the arc flame is shown. With refractive indices [*at* λ=1.55μ*m*] of core and claddings of two constituent identical fibers as 1.4580 and 1.4551respectively at no discharge, the theoretical refractive indices at the positions of the coupler waist close to arc flame and away from the arc flame (here claddings as shown in Fig.6) are n_{11}=1.45489628 and n_{61}=1.45506071, respectively, for discharge number D=1, whereas the corresponding values are n_{17}=1.45367460 and n_{67}=1.45482472 respectively, for discharge number D=7 . Effective core diameters and

core dopant diffusion around the coupler waist are considered for the analysis of the splitting ratio (*SR*) of the couplers. The flatness of *SR* values with λ improves with the lower values of effective core radius a_{eff} and for D=3 variation due to a_{eff} becomes small. For repeated discharge, at D=4 with a_{eff}=2.2μm and separation between two cores (h)=13.0μm, theoretically maximum S.R. variations were obtained as 0.67dB and 4.7dB , when the effective coupling lengths (L) were 4750.0μm and 6250.0μm respectively.

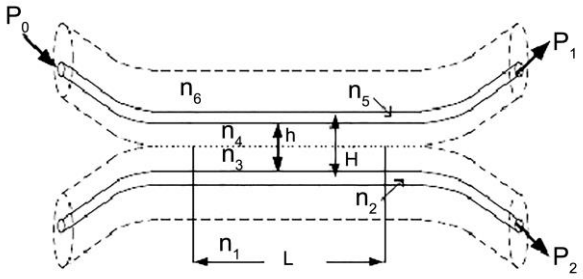

Fig. 1. A fused 2×2 fiber coupler with different refractive indices around the coupler waist.

2. Fabrication of 2×2 fused couplers

2×2 fused fiber couplers having a coupling region of length L were fabricated by fusing and tapering a pair of conventional single-mode fibers using a ceramic heater. The fibers were twisted together, melted, and pulled so they got fused together over an effective coupling length L , as shown in Fig.1. The cross section at the coupler waist assuming two cores with effective core radius a_{eff} surrounded by cladding is shown in Fig. 6. The core dopant impurities may diffuse into the nearby Claddings at the fusing temperature so that there will be refractive profile in the cores. The inset of Fig. 6 shows different core layers of the coupler waist, when the refractive index becomes higher towards the center of the core. The cross-sectional shapes of the waist were controlled by heater temperature and duration of heating. The heater temperature of 1480 ^oC -1550 ^oC was maintained during fusing and elongating, and cooled more slowly than the fiber drawing process [7,9]. The fictive temperature of the couplers was kept around 1480 ^oC or less, so that glass structures were rearranged and assumed refractive index around the coupler waist unchanged, when n_2=n_5 and n_1=n_3=n_4=n_6 . Then the average propagation constants $\beta_1$and β_2 of the two fibers in the coupling region can be assumed same and thus the difference between them $\Delta\beta=\beta_1-\beta_2=0$.

For a coupler fusing well with coupling strong, we can get enough coupled power to get SR ≈30 dB at λ=1.50μm, when the coupler waist was found relatively thick. Typical effective coupling length L ≈ 4.28$mm$when the elongation length was about8.26mm.

3. Characteristics of 2×2 symmetric couplers ($\Delta\beta=\beta_1-\beta_2=0$)

The core diameters of the fused fiber couplers are reduced to $2a_1$ around the coupler waist when the two single mode fibers of diameter $2a$ are pulled during heating process for making the coupler, and can be expressed as

$$a_{21} = \frac{2ad}{w} \tag{1}$$

where d is the width of the coupler waist and W is the effective width of the twisted fibers after heating before pulling. Normally, $2a_1$≈1.5μm when $2a$=10μm and d=40μm .

3.1. Coupling coefficients and effective core diameter around the symmetric coupler waist

The effective core diameter $2a_{eff}$ around the coupler waist will be greater than $2a_1$ because the step-index core is converted to a graded index core as shown in the inset of Fig. 6 assuming diffusion of core impurities to the cladding during heating and pulling process for fabricating the coupler. Again, the normalized frequency (V) to support a single mode in a parabolic refractive index profile (α) fiber can be expressed as [10, 11],

$$V = 2.4\left(1+\frac{2}{\alpha}\right)^{\frac{1}{2}} = 2.4\sqrt{2} \tag{2}$$

The V number for the graded index fiber with α=2 is increased by a factor of √2 on the step index case, but its factor becomes √3 over the step index for a graded index fiber with a triangular profile. This gives a core radius increased by a similar factor for the graded fiber over a step index fiber with the equivalent core refractive index and the relative refractive index difference. Again, the coupling coefficient (K_m) depends on the gap between the cores (h =H-$2a_{eff}$), $2a_{eff}$ and the operating wavelength (λ). Using Mercuse model of a symmetric directional coupler for the coupling waveguides ($2D$) model [10]

$$K_m = \frac{K_2^2\,\gamma_s \exp(-\gamma_s h)}{K_0^2\beta(n_2^2-n_s^2)\times(a_{eff}+\frac{1}{\lambda_s})} \tag{3}$$

Where

$$K_0^2 = n_2^2K_0^2 - \beta^2 \tag{4}$$

$$\gamma_3^2 = \beta^2 - n_2^2K_0^2 \tag{5}$$

$$K_0 = \frac{2\pi}{\lambda} \tag{6}$$

$$\beta = K_0N \tag{7}$$

N is the effective refractive index of the waveguide. Normally, K_m increases with the increase of λ, however, the rate of increase of K_m with λ decreases for higher

values of λ. Again, K_m increases with the decrease of a_{eff} for lower values of λ but saturates or crosses at higher values of λ [8]. The plot of $K_m(\times 10^6 \mu m^{-1})$ versus wavelength λ(μ*m)* with a_{eff}=2.2μm, 2.0μm and 1.5μ*m*, h =13.0μ*m* and L=4750.0μ*m* , for the discharge number D=0 , is shown in Fig.2, when the cladding refractive indices 1.4551, $n_{cl}=n_{10}=n_{30}=n_{40}=n_{60}=1.4551$ and core refractive indices

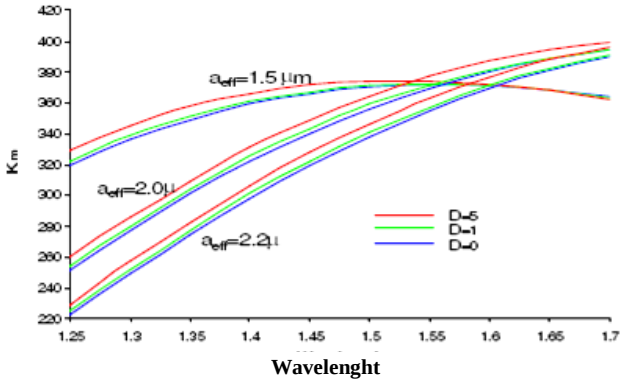

Fig. 2. Coupling coefficient K_m versus λ for different values of a_{eff} , and discharge number D.

$n_{co}=n_{20}=n_{50}=1.4580$ at λ=1.55μ*m*. Actually, D=0 represents the normal fused fiber coupler known as a symmetric coupler. The asymmetric fused fiber couplers can be made by heating the coupler waist in an asymmetric temperature profile with a given value of D forming the finite value of Δβ. However, this characteristic is required for wavelength insensitive devices to operate at higher values of λ only.

4. Coupled power and Splitting Ratio (SR) for a symmetric fused fiber coupler

The transmitted and coupled powers of a fused coupler P_1 and P_2 can be expressed from the well known coupled-mode theory, as [11]

$$P_2 = K_m^2 Sin^2(\delta_L) \quad (8)$$

$$\delta^2 = \left[\frac{\beta_1 - \beta_2}{2}\right]^2 + K_m^2 \quad (9)$$

$$P_1 = P_0 - P_2 \quad (10)$$

$$SR = 10\log_{10}\left(\frac{P_1}{P_2}\right) \quad (11)$$

where P_0 is the input power, β_1 and β_2 are the average propagation constants of the two fibers in the coupling region, K_m is the average coupling coefficient and L is the effective coupling length. *SR* is the splitting ratio (*dB*) of the output arms of the coupler. Fig. 3 shows the theoretical curves of wavelength versus Splitting Ratio for different values of a_{eff} with the fixed value of h =13.0μ*m* and 14.0μ*m* keeping the value of effective coupling length L=4750μ*m* fixed for each case when the coupler was not heated in the asymmetric temperature profile. Figure also shows that the *SR* of a symmetric coupler is completely wavelength sensitive for the particular values of physical parameters (L, h & a_{eff}) of the couplers.

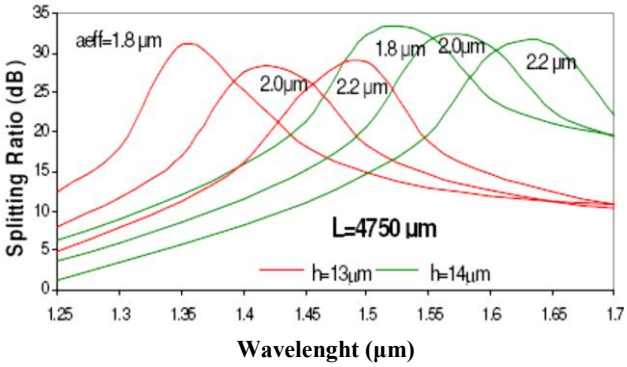

Fig. 3. Wavelength (μm) verses Splitting ratio (dB) of a symmetric coupler for different values of effective core radius with the corresponding h (μm) for L =4750μm.

It is observed that for h=13.0μ*m* and a_{eff}=1.8μm maximum splitting ratio 30.92*dB* at λ=1.35μ*m*, decreases gradually to 10.87*dB* at λ=1.70μ*m*. When a_{eff} is changed to 2.0μ*m* , peak value of *SR* shifts to λ=1.425μ*m* with the value of 28.00*dB* and decreases slowly with the increase of wavelength. For a_{eff} =2.2μm, peak value of *SR* is 28.83*dB* at λ=1.50μ*m* with a sharp fall to a value of 18.75*dB* at λ=1.55μ*m*.Other characteristic curves for the set of parameters h=14.0μ*m* with a_{eff} =1.8μ*m*, 2.0 μ*m*, 2.2μ*m* are also shown in Fig.3. It is observed that the peak values of *SR* shift towards higher wavelength as a_{eff} increases. Thus, all *SR* curves for a symmetric coupler are wavelength sensitive for the variation of either h, or a_{eff} keeping the coupling length fixed. However, the peak values of *SR* can be made approximately at the same wavelength (λ_p) by choosing a set of value of a_{eff} and L with the fixed value of h , but *SR* will be wavelength dependent.

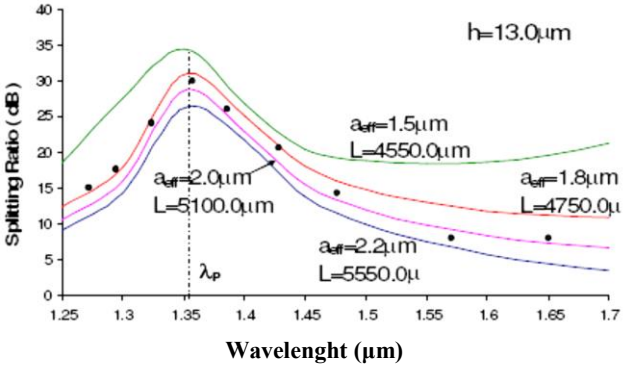

Fig. 4. Wavelength (μm) verses Splitting ratio (dB) of a symmetric coupler waist for different values of effective core radius with the corresponding coupling length L .

Fig. 4 shows the theoretical curves of wavelength versus Splitting Ratio for different combination of a_{eff} and L at a constant value of h=13.0μm when the peak value of SR increases with the decrease of both L and a_{eff} at λp≈1.35μm. It is important to note that the combination of higher values of L with the higher values of a_{eff} arises for the fabrication of 2×2 couplers during heating and pulling process. For the higher values of L , though the core radius 'a' decreases, but a_{eff} increases due to formation of graded index core from its initial step-index fiber along the coupler waist as discussed above. Table-1 shows the increase of SR values with the decrease of a_{eff} and also the lower values of L at a constant value of h .

Table-1

Space between two cores , h =13.0μm	
Combination of a_{eff} and L	Peak value of SR (dB)
1.5μm, 4550.0μm	34.59
1.8μm, 4750.0μm	30.92
2.0μm, 5100.0μm	28.61
2.2μm, 5550.0μm	26.31

5. Experiments to measure the characteristics of the symmetric coupler

Fig. 5 is a schematic diagram of the experimental setup used to measure the characteristics of the 2×2 fused fiber couplers. We used a stabilized tunable Laser diode source of wave length range λ=1.25μm to λ=1.70μm and line width 10GHz . An optical fiber was used to butt couple the source to the waveguide. The core refractive index of the fiber was taken higher than that of a standard telecommunication fiber for single mode operation known as coupling fiber, which minimizes the Fresnel reflections loss between the coupling fiber and the 2×2 coupler. The core diameter of the fiber was slightly greater than the coupling fiber so that the maximum power could be launched into the coupler. Output power was detected by a movable Germanium p-i-n detector at the other end of the coupler through the focusing lens. Detected power was amplified by a chopper stabilized trans impedance -type preamplifier. The minimum detectable power, of the order of 100 pW , was obtained by proper shielding of the receiver. We chose the couplers which were fabricated with effective coupling length L=4750.0μm having a_{eff} ≈1.8 μm by controlling the heating and pulling process as discussed above. The average experimental results obtained by using the set-up of Fig. 5 without arc flame, show the SR values for different wavelengths for D=0 which almost agree with the theoretical curves of Fig.4.

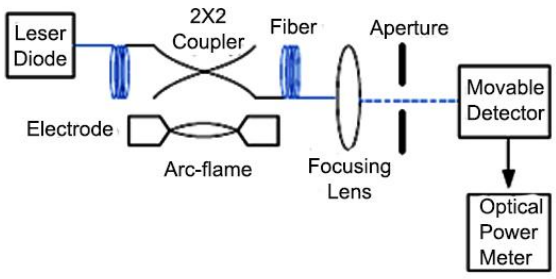

Fig. 5. Schematic diagram of the experimental set-up.

6. Coupled power and Splitting Ratio (SR) for an asymmetric fused fiber coupler

($\Delta\beta=\beta_1-\beta_2\neq0$)

6.1. Coupler waist in asymmetric temperature profile and glass structure variation

Placing the coupling region away from the center of the arc flame as shown in Fig. 6 in an arc discharge, the coupler waist was heated unequally due to temperature profile of the flame. The temperature of the arc flame was controlled by arc current I_a flowing between the arc electrodes [8]. The temperature of the arc flame decreases with increasing distance from the center of the flame. The coupler waist having two cores and four claddings and placing the same in the temperature profile gets heated at different temperatures depending on the profile parameters. The temperature of the coupler waist was kept 2000 ºC by controlling I_a with short flame duration of few ms. The variation of peak arc temperature with arc current was measured experimentally using optical pyrometer under the condition of fixed electrode separation ,which is shown in Fig. 7.Heating the glass at such higher temperature than T_F (glass fictive temperature) [7,9] and cooled rapidly of ms order (much shorter than structural relaxation time), the glass structure reaches an equilibrium state when the density is decreased greatly by rapid solidification process.

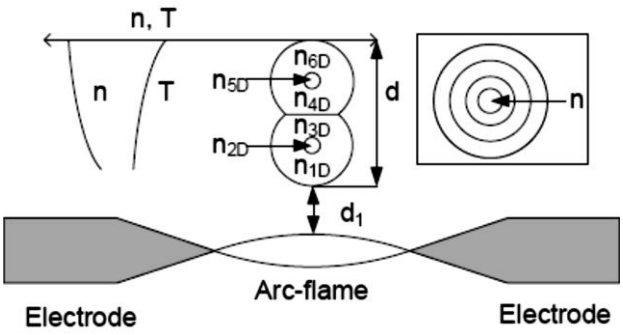

Fig. 6. Schematic diagram of heating the coupler waist unequally by arc discharge to obtain refractive index profile. The inset is the amplified portion of the cores.

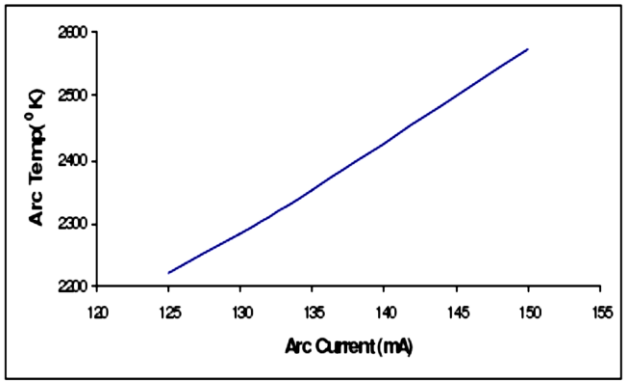

Fig.7. Variation of Arc Temperature (0K) with Arc Current (mA).

6.2. Refractive index variation around the coupler waist with repeated arc discharge

When the coupler is heated unequally by an arc discharge, the symmetric coupler becomes asymmetric as the refractive indices of cores and claddings of constituent fibers change unequally and the cross sectional view is shown in Fig.6. The plot $K_m(\times 10^6 \mu m^{-1})$ versus wavelength λ (μm) with a_{eff}=2.2µm,2.0µm and 1.5µ*m*, *h*=13.0µ*m* and *L*=4750.0µ*m* , for discharge number *D*=1 and *D*=5 are shown in Fig.2. If the operating wavelength remains unchanged for each discharge, then we get the refractive index profile along the coupler waist as shown in Fig.8.

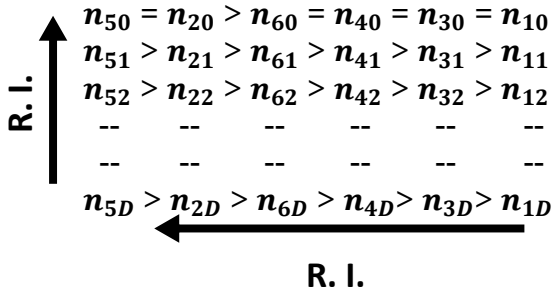

Fig. 8. Variation of refractive indices along the coupler waist with the discharge number D.

D=0 ,1,2 .... *D* is the number of arc discharge and n_{5D}, n_{2D}, are refractive indices of the cores at distant and nearer from the arc flame, respectively.n_{6D}, n_{4D}, n_{3D} and n_{1D} are the refractive indices of the claddings around the coupler waist as shown in Fig.6. Typical values of the refractive indices for *D*=0,1,2 and 7 at λ=1.55µ*m* are shown in Table 2.

Table 2 shows the decrease of refractive indices for increasing number of discharge and also for the position of coupler waist close to arc flame.

Table. 2

Increase of D decreases R.I. of the coupler waist						
	1.458	1.458	1.4551	1.4551	1.4551	1.4551
	1.457 88627	1.457 87334	1.4550 6071	1.454 98621	1.454 97428	1.454 89628
	1.45 777256	1.457 74748	1.455 02143	1.4548 7243	1.4548 4857	1.454 69260
	--	--	--	--	--	--
	--	--	--	--	--	--
	1.45 720412	1.457 11639	1.454 82472	1.4543 0366	1.4542 2018	1.453 67460
R.I. decreases along the coupler waist closer to the arc →						

6.3. Refractive indices around coupler waist with and without core dopant diffusion

Since the refractive index of glass is directly proportional to its density, hence there will be a refractive index profile in the coupler waist when the refractive index increases along the distance away from the center of the arc flame, as shown in Fig.6. The profile parameter (*D*1) controls the refractive indices of the cores and cladding of the couplers. (*D*1) depends on I_a , duration of heating (*t*), and the placing the coupler waist in the arc flame (d_1) when d_1 is the distance between the edge of the arc flame and the edge of the coupler waist. We can express the following equation for refractive index variation of claddings as

$$n_i = n_{6D} e^{-1y^2} \qquad (12)$$

where *y* is the distance from the farthest edge of the coupler waist, and it increases towards the arc flame and the cladding refractive indices n_i increase with the increase of 'i' values. The refractive indices of core will be Rn_i , where R = n_{co}/n_{cl} . If the discharge is repeated then n_i will decrease further assuming as $n_{6D} - k_d D$, where *D* is the number of arc discharge and k_d is a constant depending on arc condition and position of the coupler waist.

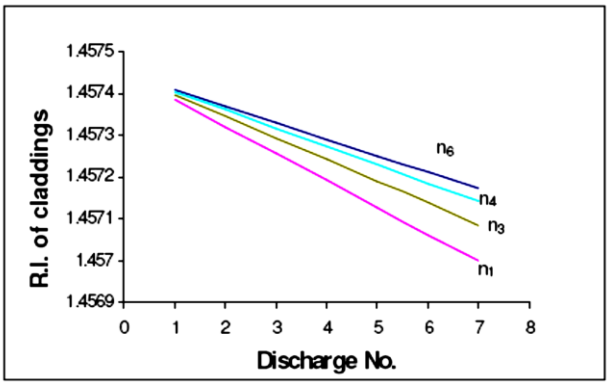

Fig. 9. Plots of refractive index of claddings around the coupler waist versus number of discharge D.

The plots of refractive indices of claddings n_i versus D for a_{eff}=2.2μm, h=13.0μm, L =4750μm are shown in Fig.9 for a typical value of D1and k_d . For a fixed value of D, the refractive index at different positions of the claddings of the coupler waist for D= 1, and 7 are shown in Fig.10, d is the width of the coupler waist, where relative position of n_{6D} is d/8. The refractive indices around The coupler waist discussed above are calculated without considering core impurity diffusion in the cladding region.

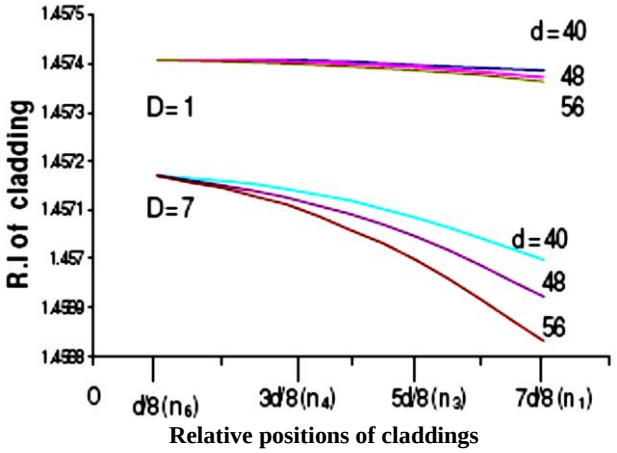

Fig. 10. Refractive indices of claddings decrease closing to arc flame of coupler waist, and also decrease with discharge numberD.

6.4. Core dopant diffusion

For an arc flame of temperature $T > 20000C$ around the coupler waist it is expected that the core dopants required to obtain core refractive index high will diffuse around cladding. The dopant concentration N (x,t) will decrease with the increase of t and the diffusion constant D_f following the Gaussian distribution as [12].

$$N(x,t) = \frac{N_d}{(\prod D_f t)^{1/2}} e^{\left(\frac{-x^2}{4tD_f}\right)} \qquad (13)$$

where x, N_d are the distance from the core edge to the nearby claddings and the average dopant concentration of the core of coupler waist, respectively. The typical value of D_f as a function of temperature for the relevant core impurity element in silica glass is shown in Fig. 11. It shows that for the typical arc discharge temperature ≈2353^0 K, D_f is of the order of 4×10^{-7}cm^2/sec for Al_2O_3 and 3.6×10^{-7}cm^2/sec for GeO_2. Again, the refractive index of the core n_{co} depends on the choice of dopant concentration (*mole%)* and a typical graph is shown in Fig. 12. For repeated arc discharge with t =5ms, D=5 diffusion constant (D_f) is 9×10^{-7} cm^2sec and dopant concentration $N_d \approx 1.07\times10^{21} cm^{-3}$ for GeO2 dopant. As a result of core dopant diffusion refractive index n_{2D} decreases by 0.027% and n_{5D} decreases by ≈ 0.016% from their initial value at D= 0 .

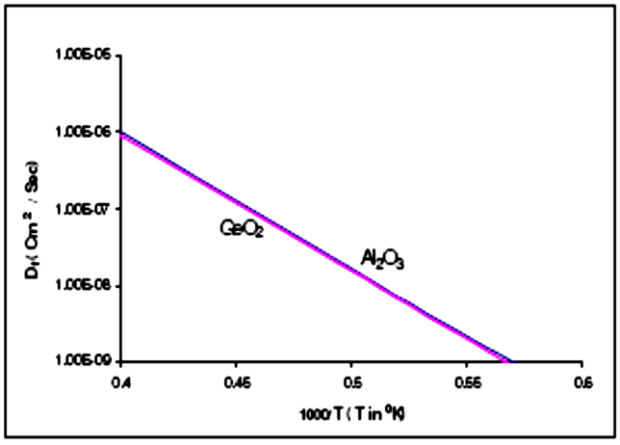

Fig. 11. Diffusion constant f D versus temperature for the relevant core impurity element in silica glass.

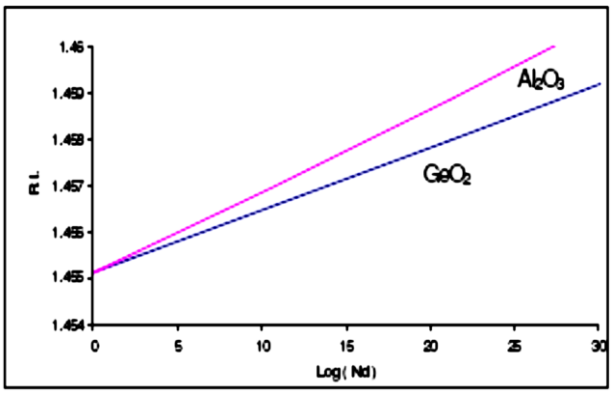

Fig 12. Refractive index versus dopant impurity N_d of the typical optical glass fiber.

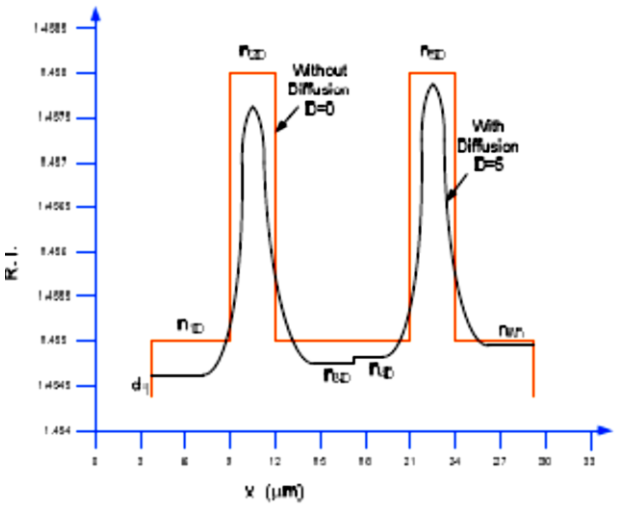

Fig. 13. Refractive profile around the coupler waist considering core impurity diffusion.

The change of refractive index of core due to diffusion of Al_2O_3 dopant into claddings is shown in Fig. 13. The diffusion nature of dopant from the core to the cladding is also shown in the figure. The refractive index

profile of t 0.14he cores and claddings around the coupler waist with and without diffusion for D= 0 and 5 is shown in the figure.

6.5 Propagation constants β_1 and β_2 of the modes of two fibers around coupler waist

The variation of ni around the coupling zone due to unequal heating creates the difference between the propagation constants of the two modes when there will be the phase mismatch and this difference between two propagation constants ($\Delta\beta$) increases with the increase of k_d and D, and also depends on the value of $D1$. The plot of $\Delta\beta(\times10^6)$ versus $D1(\times10^7)$ is shown in Fig. 14(a) for λ=1.35μm indicating increase of $\Delta\beta$ increase of $D1$ for $D=1$. Again increase of $\Delta\beta$ with repeated discharge for the same wavelength is shown in Fig. 14(b) considering $D1 = 0.14\times10^{-7}$ for $D=1$. However, we can obtain another value of $\Delta\beta$ value of $D1$ for D=1 or other value of D.

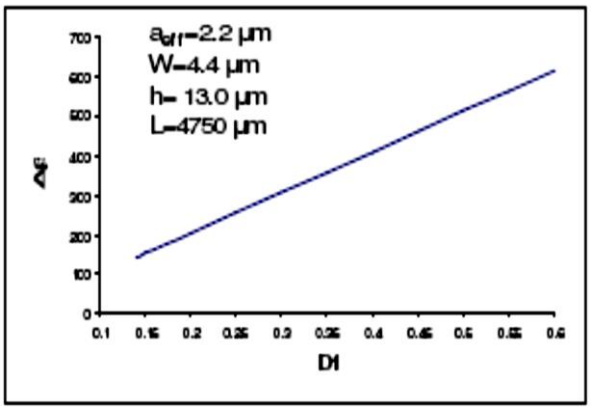

Fig. 14(a). Plots of difference of propagation constants $\Delta\beta$ for two modes versus profile parameter D1.

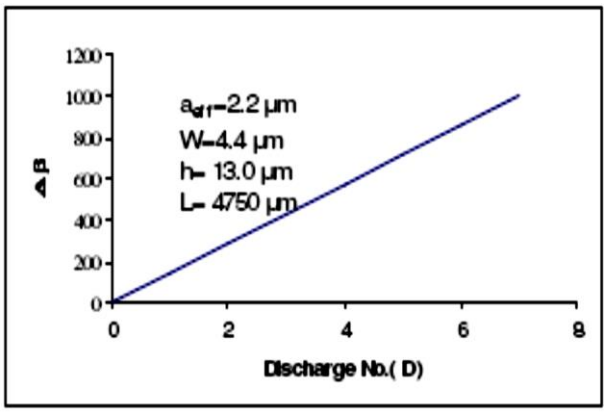

Fig. 14(b). Plots of difference of propagation $\Delta\beta$ for two modes versus discharge no.D.

6.6 Wavelength sensitive/insensitive couplers

The theoretical plots of splitting ratio (SR) versus wavelength for different conditions of the coupler waist are shown in Fig. 15. The wavelength insensitivity characteristic is observed when a_{eff} =2.2µm,W =4.4µm, h=13.0µm, L=4750µm for discharge number D4 as shown in Fig. 15 (c). However, the other conditions show the wavelength sensitivity characteristics as shown in Figs. 15 (a) and 15(b).

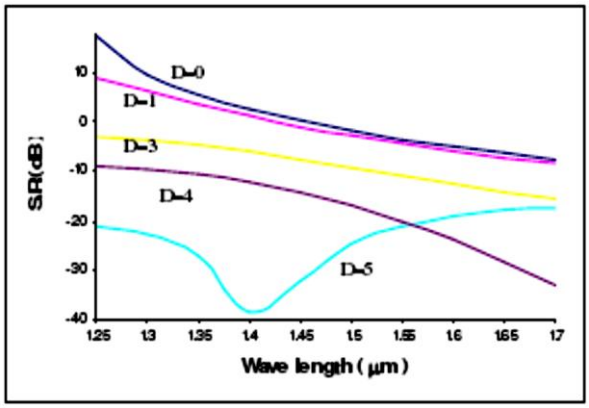

Fig. 15(a). Splitting Ratio vs wavelength for a_{eff} =2.2µm, W=4.4µm, h=12.0µm, L=6250µm.

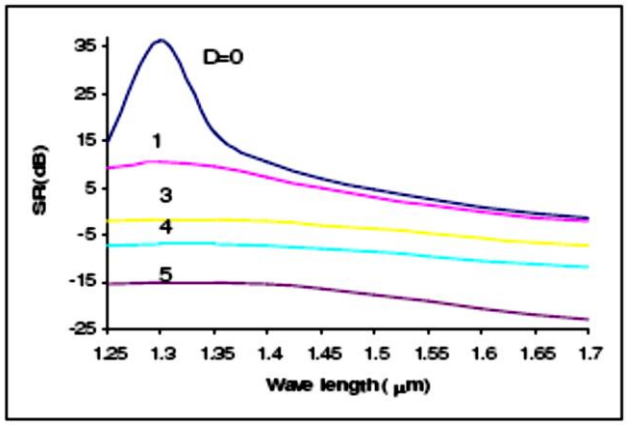

Fig. 15(b). Splitting Ratio vs wavelength for a_{eff} =2.2µm, W=4.4µm, h=13.0µm, L=6250µm.

7. Experiment and results – wavelength insensitive coupler characteristics

The wavelength insensitive fused fiber coupler was achieved by first fabricating a 2×2 coupler of a_{eff}=2.2µm, coupling length (L)=4750µm and h=13.0µm by fusing and elongating a pair of conventional single-mode fibers using a ceramic heater as mentioned before, and then the coupler waist was placed 50µm-100µm away from the edge of the arc flame as shown in Fig. 6 to obtain the temperature profile for unequal heating.

We carried out the experiment using the set-up as shown in Fig. 5. The arc was repeatedly discharged without moving the coupler and electrodes. The discharge current and discharge time were 125mA 140mA and 4.5ms respectively, producing arc temperature of near about 2200^0 C at the centre of the arc. The transmitted and the coupled powers were measured by optical power meter after each µ discharge for each wavelength ranging from 1.25µm to 1.70µm.Experimental results are the average values of SR obtained at different values of wavelengths and are shown in Fig. 15(c).

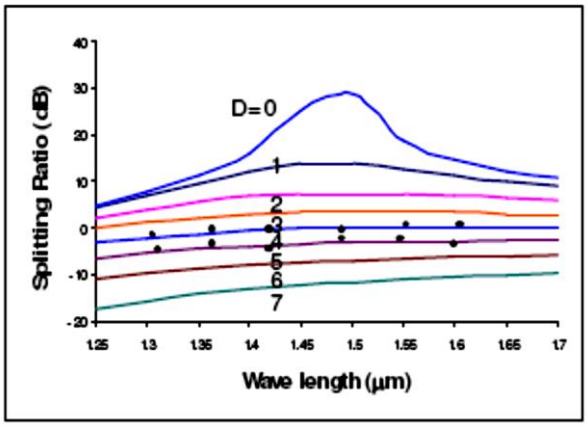

Fig. 15(c). Splitting ratio SR versus λ of the well fused coupler for different values of discharge D when a_{eff} =2.2μm, W=4.4μm, h=13.0μm, L=4750μm

This figure also shows the plots of splitting ratio SR versus λ for different values of discharge number D with the profile parameter $D1 = 0.14 \times 10^{-7}$ following equations (3) and (8) – (11). It shows that the experimental result agrees with the theoretical curves of Fig. 15(c), when *D is 4*- 5 indicating wavelength insensitive coupler characteristics. This result also proves that the coupling length is ≈4750.0μ*m*, when a_{eff} =2.2μm and *h*=13.0μ*m* comparing with the theoretical curves of Fig. 15(c).

8. Conclusion

We demonstrated the fabrication of 2×2 wavelength insensitive fused fiber couplers using a temperature profile condition in the coupler waist obtained by arc discharge. The coupler waist was placed away from the arc flame to heat the coupler waist unequally. The variation of refractive indices of two cores and four claddings of two fibers around the coupler waist depending on both the number of arc discharge and the position of the coupler waist from the centre of the arc flame is studied. It shows decrease of refractive indices both for increasing number of discharge and the position of coupler waist close to arc flame. A theoretical model for splitting ratio (*SR)* versus wavelength (λ) with repeated discharges considering temperature profile parameters is developed using coupled mode theory. Diffusion of the dopant core impurities is considered for the analysis of *SR* . The theoretical curves are compared with the experimental results. The wavelength flattened range is from 1.35μ*m* to 1.70μ*m* with maximum *SR* variation of 1.32*dB* for discharge number *D*=4 ,when (*h*=13.0μ*m* and *L*=4750.0μ*m*) . However, this value becomes 5.05*dB* for the same values of coupler waist parameters and discharge number, but changing coupling length (*L*) to 6250.0 μ*m*.

Acknowledgement

The Authors wish to thank NSHM Knowledge Campus, Durgapur for providing excellent research facilities. Moreover, Arindam Biswas is grateful to Professor (Dr.) P. K. Bose, Campus Director, NSHM Knowledge Campus, Durgapur, for motivating to carry out the present work.

References

[1] J. D. Minelly, C. D. Hussey, Electron. Lett. **23**(20), 1087 (1987).
[2] K. Morishita, T. Tahara, Electron. Lett. **27**(13), 1200 (1991).
[3] F. Gonthier, D. Ricard, S. Lacroix, J. Bures, Opt. Lett. **16(**15), 1201 (1991).
[4] Y. Takeuchi, J. Noda, IEEE Photon. Technol. Lett. **4**(5), 465 (1992).
[5] P. F. O'Sullivan, C.D. Hussey, Electron. Lett. **33**(4), 321 (1997).
[6] C. D. Hussey, T. A. Birks, Electron. Lett. **24**(17), 1072 (1988).
[7] K. Morishita, N. Ohta, J. Lightw. Technol. **26**(13), 1915 (2008).
[8] B. K. Ray, A.Das, A. K.Das, IEEE 7th Inter. Con. WOCN2010, 4-6 Sept. 2010 Colombo, Sri Lanka.
[9] A.K. Das, S. Bhattacharyya, IEEE Journal of Lightwave Technology **3**(1), 82 (1985).
[10] D. Mercuse, J. Lightw. Technol. **5**(1), 113 (1987).
[11] A. K. Das, Applied Optics **42**(7), 1236 (2003).
[12] J. Millman, C. C. Halkias, Integrated Electronics, McGraw- Hill, Inc. New York, 1972.

*Corresponding author: mailarindambiswas@yahoo.co.in